Proceedings of the ASME 2010 3rd Joint US-European Fluids Engineering Summer Meeting and 8th International Conference on Nanochannels, Microchannels, and Minichannels
FEDSM-ICNMM2010
August 1-5, 2010, Montreal, Canada

FEDSM-ICNMM2010-31183

DYNAMICS OF FLOW AROUND A CYLINDER OSCILLATING IN-LINE FOR LOW REYNOLDS NUMBERS

L. Baranyi
Dept of Fluid & Heat Engineering, University of Miskolc
Miskolc, Hungary
E-mail: arambl@uni-miskolc.hu

K. Huynh
Department of Mechanical Engineering
Ecole Polytechnique
Montréal, QC, Canada, H3C 3A7
Kenny.huynh@polymtl.ca

N. W. Mureithi
BWC/AECL/NSERC Chair of Fluid-Structure Interactions
Department of Mechanical Engineering
Ecole Polytechnique
Montréal, QC, Canada, H3C 3A7
njuki.mureithi@polymtl.ca

ABSTRACT

This study builds on an earlier study of low-Reynolds number flow about a cylinder forced to oscillate in-line with the main flow, which found vortex switches at some oscillation amplitude values. Here we extend the Reynolds number domain to Re=60-350, utilize a computational domain characterized by R_2/R_1=360, and do computations at two frequency ratios of f/St_0=0.8 and 0.9. Computations were carried out using a thoroughly tested finite-difference code. Some results were compared with those obtained by Ansys CFX, and good agreement was found.

When plotted against oscillation amplitude, rms and time-mean values of force coefficients revealed a shift toward lower amplitude with higher Re. Findings for the effect of frequency ratio are similar.

Where vortex switches occurred, a pre-and post-jump analysis is carried out. POD analysis of the cylinder wake flow field is employed to reveal the detailed wake dynamics as the forcing parameters are varied. The analysis provides further details on the transition of the dominant wake modes in response to the symmetry breaking bifurcation underlying the vortex switches observed in the simulations.

Keywords: circular cylinder, in-line oscillation, POD, symmetry-breaking bifurcation

INTRODUCTION

Flow around oscillating cylinders is of both practical and academic interest, and has thus been widely studied. Structures exposed to wind or waves can oscillate, which can have consequences in terms of vibration, stresses and wear, noise, and even the viability of the structure. Flow-structure interaction is complex in any case, and particularly so when the bluff body is also in motion. If a cylinder is in forced motion, then the vortex shedding patterns are affected by factors such as cylinder forcing frequency and the amplitude and direction of oscillation, in addition to the Reynolds number of the flow.

At low Reynolds numbers, studies have identified vortex switches for cylinders in motion. Williamson and Roshko (1988) determined experimentally a map of vortex shedding modes for a transversely oscillating cylinder. Forced oscillation studies such as those of Blackburn and Henderson (1999) for Re=500, Kaiktsis et al. (2007) for Re=200, and Lu and Dalton (1996) for Re=185 have found vortex switches in transverse oscillation at frequency ratios over 1. Baranyi (2008a), investigating orbital cylinder motion, found sudden vortex switches (referred to as jumps) when varying the amplitude of transverse oscillation for frequency ratios below 1.

For in-line oscillation, an experimental study by Cetiner & Rockwell (2001) was carried out at medium Reynolds numbers over a frequency ratio range of 0.44 to 3. Al-Mdallal et al. (2007) investigated a similar frequency ratio range numerically at Re=200, finding vortex switches. A low-Reynolds number numerical study (see Baranyi, 2009) also identified vortex switches for in-line oscillation against oscillation amplitude and also against frequency ratio ranging from 0.76 to 0.94, Baranyi (2008b). At some critical parameter values, flow pattern switched into a mirror image. Konstantinidis et al. (2005) report on particle image velocimetry measurements obtained in the forced wake of a circular cylinder in an incident flow with low-amplitude periodic velocity oscillations superimposed upon it.

This case is equivalent to that of a cylinder forced to oscillate in-line with a steady incident flow.

Another numerical study at Re=200 and frequency ratio 1 is Mureithi et al. (2009). Complex dynamics including quasi-periodicity, torus doubling and chaos were uncovered by the authors. A low order discrete model was developed based on symmetry-equivariance theory. The required numerical parameters for the model were determined via a POD decomposition of the temporal velocity field. The resulting simple model was found to capture the observed wake dynamics, qualitatively predicting the sequence of bifurcations found in the numerical computations.

This numerical study investigates the effect of oscillation amplitude on the flow around a circular cylinder oscillating in-line at 9 different Reynolds numbers, ranging from Re=60-350, at two frequency ratios of 0.8 and 0.9. In addition to pre- and post-jump analysis, POD analysis is utilized in order to identify the detailed wake dynamics.

NOMENCLATURE

$A_{x,y}$ amplitude of oscillation in x or y directions, respectively, non-dimensionalized by d
C_D drag coefficient, $2F_D/(\rho U^2 d)$
C_L lift coefficient, $2F_L/(\rho U^2 d)$
C_{pb} base pressure coefficient
d cylinder diameter (m)
F_D drag per unit length of cylinder (N/m)
F_L lift per unit length of cylinder (N/m)
f oscillation frequency, non-dimensionalized by U/d
f_v vortex shedding frequency, non-dimensionalized by U/d
p pressure, non-dimensionalized by ρU^2
R radius, non-dimensionalized by d
Re Reynolds number, Ud/ν
St non-dimensional vortex shedding frequency, $f_v d/U$
t time, non-dimensionalized by d/U
tq torque coefficient, torque of shear on cylinder surface, non-dimensionalized by $\rho U^2 d^2$
U free stream velocity, velocity scale (m/s)
u,v velocities in x,y directions, non-dimensionalized by U
x,y Cartesian co-ordinates, non-dimensionalized by d
ν kinematic viscosity (m^2/s)
ρ fluid density (kg/m^3)
τ shear stress, non-dimensionalized by ρU^2
ω vorticity, $\partial v_y/\partial x - \partial v_x/\partial y$, non-dimensionalized by U/d

Subscripts

D drag
fb fixed body
L lift
rms root-mean-square value
v vortex shedding
x, y components in x and y directions
0 for cylinder motion; for stationary cylinder at same Re; values on the wall
1 on the cylinder surface
2 on the outer boundary of the physical domain

COMPUTATIONAL METHOD

A non-inertial system fixed to the cylinder is used to compute two-dimensional low-Reynolds number unsteady flow around a circular cylinder placed in a uniform stream and forced to oscillate in in-line direction. The governing equations are the non-dimensional Navier-Stokes equations for incompressible constant-property Newtonian fluid, the equation of continuity and the Poisson equation for pressure. On the cylinder surface, no-slip boundary condition is used for the velocity and a Neumann type boundary condition is used for the pressure. At the far region, potential flow is assumed. Potential flow is assumed as an initial condition except for the cylinder surface, where zero velocity is used. The authors are aware of the fact that the potential flow assumption is not valid for the narrow wake domain on (R_2), shown in Fig. 1. Since numerical analysis and tests showed that this simplifying assumption results in only a small distortion of the velocity field near the outer boundary wake region (Baranyi, 2008a), this simplified boundary condition is kept.

Boundary-fitted coordinates are used to impose the boundary conditions accurately. The physical domain, bounded by two concentric circles, can be mapped into a rectangular computational domain where the spacing is equidistant in both directions (see Fig. 1). In the physical domain logarithmically spaced radial cells are used, providing a fine grid scale near the cylinder wall and a coarse grid in the far field. The governing equations and boundary conditions are also transformed into the computational plane and are solved by finite difference method. Space derivatives are approximated by fourth-order central differences, except for the convective terms for which a third-order modified upwind scheme is used. The Poisson equation for pressure is solved by the successive over-relaxation (SOR) method. The Navier-Stokes equations are integrated explicitly and continuity is satisfied at every time step. For further details see Baranyi (2008a).

The 2D code developed by the author has been extensively tested against experimental and computational results for a stationary cylinder (Kravchenko et al., 2004 and Chakraborty et al., 1999) and computational results for cylinders oscillating in transverse or in in-line directions or following a circular path, including Lu and Dalton (1996), Al-Mdallal et al. (2007) and Didier and Borges (2007) with good agreement being found, (Baranyi, 2008a). For this study the dimensionless time step was 0.0005. Polar co-ordinates were used, the relatively large computational domain was characterized by R_2/R_1=360, and the number of grid points was 481x451. The minimal mesh size next to the cylinder surface was $\Delta R_{min}/d$=1.00658; the ratio of consecutive mesh sizes was constant at $\Delta R_{i+1}/\Delta R_i$=1.013166).

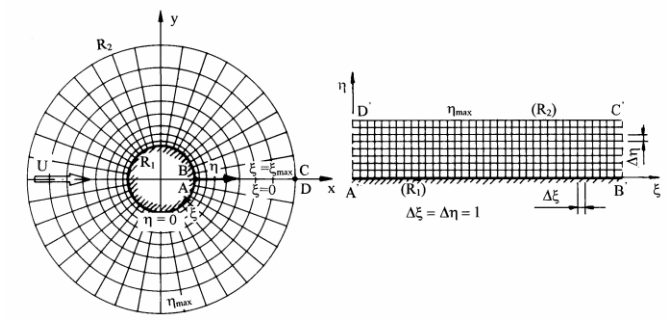

Figure 1. Physical and computational domains

In this study, computations for a cylinder oscillated mechanically in in-line direction were carried out at nine Reynolds numbers (Re=60, 80, 100, 120, 160, 220, 250, 300, and 350), a range within the limits of simulation by a 2D code for an oscillating cylinder. The non-dimensional frequency of oscillation $f_x=f$ was set at $0.8St_0$ and $0.9St_0$ values, where St_0 is the non-dimensional vortex shedding frequency, or Strouhal number, for a stationary cylinder at that Reynolds number. This selection of f ensures synchronization or lock-in at moderate A_x oscillation amplitude values. The values used in this study are taken from Posdziech and Grundmann (2007) and Norberg (2003). In this study, the flow was considered to be locked-in when the vortex shedding frequency f_v is equal to the frequency of cylinder oscillation f. For in-line oscillation, lock-in was found earlier in the vicinity of the natural vortex shedding frequency f_{v0}, as well as the double of this frequency (Baranyi, 2008a; Didier and Borges, 2007). Here the first, narrower lock-in domain has been chosen. To create a more manageable scope of investigation, only locked-in cases were considered in this study.

Time-mean (TM) and root-mean-square (rms) values of lift (C_L), drag (C_D) (without inertial forces), base pressure (C_{pb}) and torque (tq) coefficients were evaluated and plotted against the oscillation amplitude. Computations are performed at a fixed Re and f values with amplitude of oscillation as the independent variable.

Here the torque coefficient tq (positive in counter-clockwise direction) is determined from the torque of the shear acting on the cylinder:

$$\mathrm{tq} = -\int_0^{2\pi} \tau_0(\psi) R_1^2 \mathrm{d}\psi = -\frac{1}{4}\int_0^{2\pi} \tau_0(\psi)\mathrm{d}\psi = \frac{1}{4\mathrm{Re}}\int_0^{2\pi} \omega_0(\psi)d\psi$$

where ψ is the polar angle, τ_0 and ω_0 are dimensionless wall shear stress and vorticity, respectively. Here the well-known relationship between dimensionless shear stress and vorticity on the cylinder surface of $\omega_0 = -\mathrm{Re}\ \tau_0$ was used, where Re is the Reynolds number. A similar torque coefficient is defined in Chen et al. (1995). Due to symmetry, naturally the time-mean value of torque tq, like that of the lift C_L, is zero for a stationary cylinder under lock-in conditions.

RESULTS

Computational results were obtained for 9 Reynolds numbers at two frequency ratios. Here we focus on the effects of amplitude oscillation, Re, and frequency ratio on the rms and TM of force coefficients. When a vortex switch was identified, a pre- and post-jump analysis was carried out. Time-history of lift, drag-lift limit cycle curves, and vorticity contours were plotted for amplitude values directly before and after the switch. Limit cycle curves were compared for Re=200 with those using a different computational method. For further insight into the observed wake flow bifurcation, spatial and temporal POD analysis of the velocity fields was also performed for one of the computational cases.

The Effect of Reynolds Number at $f=0.8St_0$

Figures 2-4 show the TM values of lift for the 9 Reynolds numbers investigated. In all cases, the solution switches between two so-called state curves (Baranyi, 2008a); the number and location of jumps varies. The two state curves in each set of curves, for lift coefficient and torque, are mirror images of each other. This, coupled with the existence of a critical amplitude beyond which the pair of curves appears strongly suggests that a pitchfork bifurcation underlies the resulting flow asymmetry. At lower Re, such as Re=60, a higher amplitude is needed to trigger a switch between state curves (see Fig. 2). With increasing Re the locked-in domain shifts towards smaller amplitude values, especially in Figs. 2 and 3.

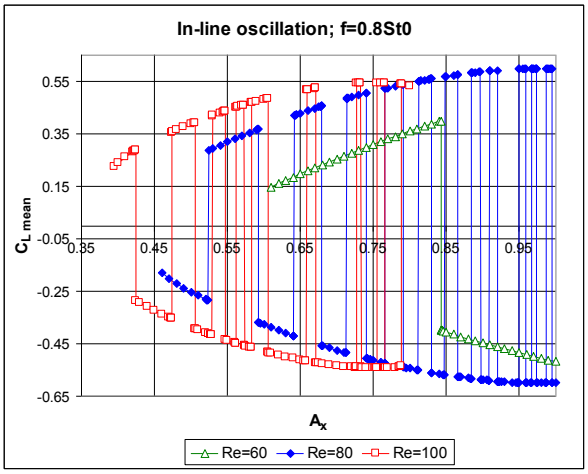

Figure 2. Time-mean value of lift against amplitude at Re=60, 80, 100

The TM drag is shown in Figs. 5 and 6. Unlike the TM of lift, no switches are present in the locked-in domain. By increasing the Re, the curves once again shift to smaller amplitude values. At lower Re the curve is nearly linear, but curvature increases with increasing Re.

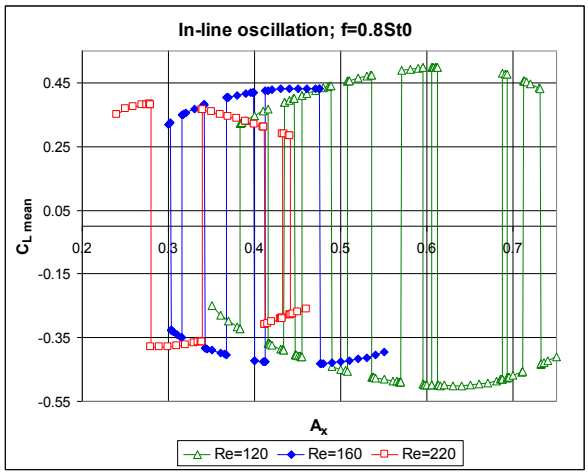

Figure 3. Time-mean value of lift against amplitude at Re=120, 160, 220

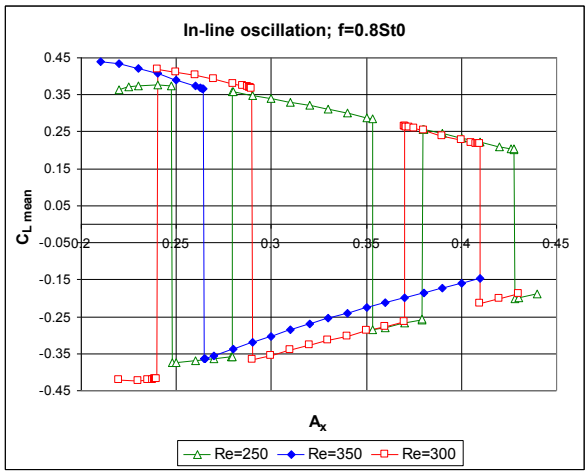

Figure 4. Time-mean value of lift against amplitude at Re=250, 300, 350

The TM of torque is shown in Fig. 7 for the four lower Re values investigated (other Re values are not shown here). The TM of torque is similar to that of lift, with both coefficients displaying shifts between state curves. The TM of base pressure behaves like the TM of drag (see Figs. 5 and 6), as do all rms values. The TM of lift and of torque are distinguished from the others by the fact that a single period includes the shedding of two vortices, rather than one, at least for a stationary cylinder. The location and number of jumps are identical to those of the corresponding curves for the TM of lift in Figs. 2 and 3. Here also the state curves are symmetrical.

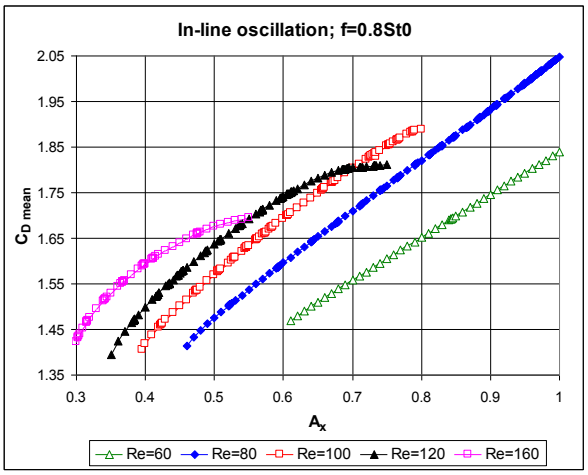

Figure 5. Time-mean value of drag against amplitude at Re=60, 80, 100, 120, 160

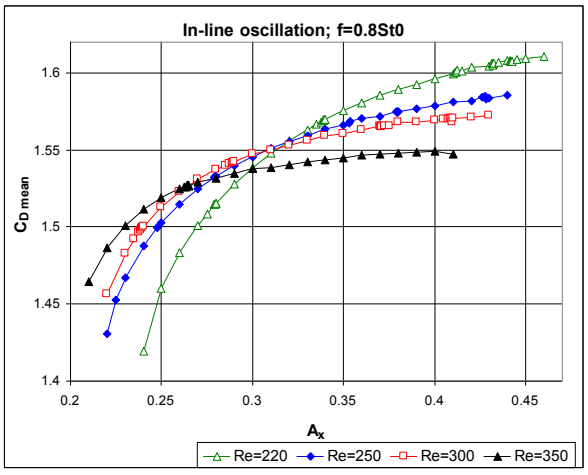

Figure 6. Time-mean value of drag against amplitude at Re=220, 250, 300, 350

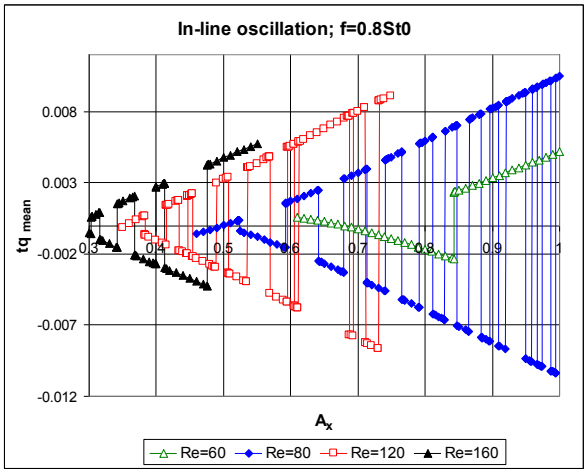

Figure 7. Time-mean value of torque against amplitude at Re=60, 80, 120, 160

The rms of drag for the lower Re values is shown in Fig. 8. The shift to lower amplitudes with increasing Re is once again visible, although the increase in curvature is less obvious.

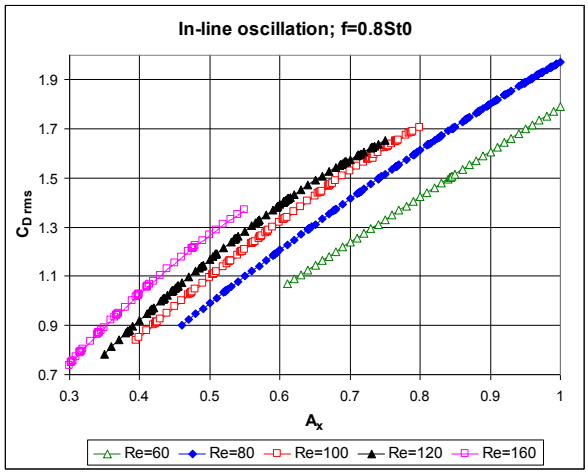

Figure 8. Rms value of drag against amplitude at Re=60, 80, 100, 120, 160

The Effect of Reynolds Number at f=0.9St$_0$

Computations were repeated for the frequency ratio of 0.9. The TM of lift is shown for five Re values (Figs. 9 and 10). As a comparison of results for Re=80 and 100 shows, at the higher frequency ratio (Fig. 9) there is a considerable shift towards lower amplitude values from results for f/St$_0$=0.8 (Fig. 2). The corresponding state curves are symmetrical. Figure 10 shows the TM of lift at higher Re, obtaining rather unusual curves that intersect each other.

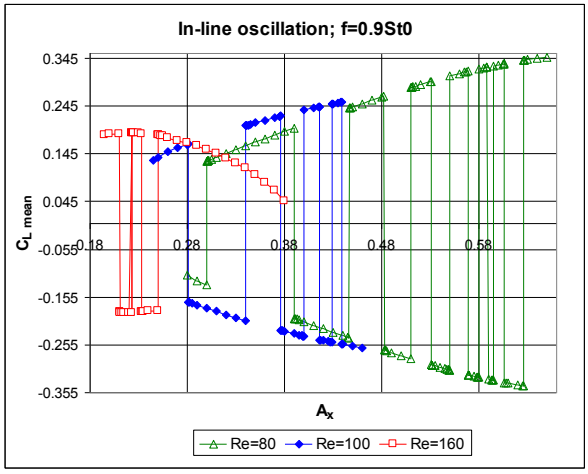

Figure 9. Time-mean value of lift against amplitude at Re=80, 100, 160

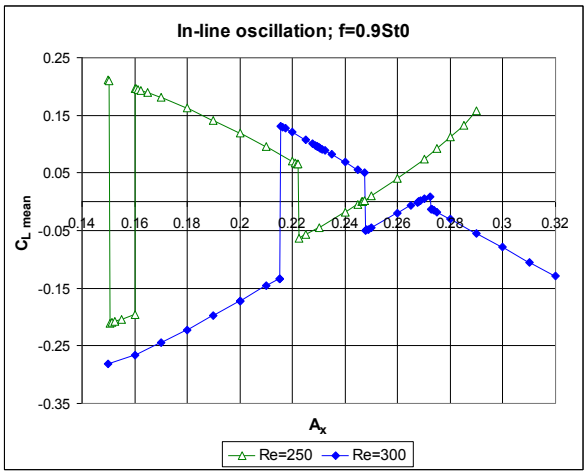

Figure 10. Time-mean value of lift against amplitude at Re=250, 300

The TM and rms values of drag are shown in Figs. 11 and 12, respectively. No switches are found, amplitude values shift down with increasing Re, and curvature increases with Re. Compared with f/St0=0.8 shown in Figs. 5, 6 and 8, the curves shift to smaller amplitude values.

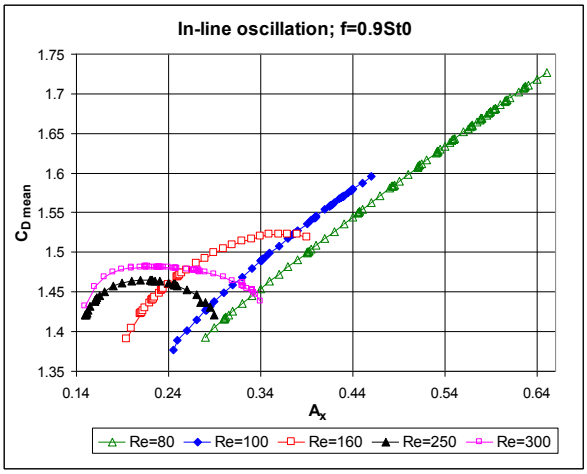

Figure 11. Time-mean value of drag against amplitude at Re=80, 100, 160, 250, 300

Figure 13 shows a comparison of two frequency ratios for Re=80. As can be seen from the figure, the curve shifted to lower amplitude values at the higher frequency ratio. Other force coefficients show a similar trend.

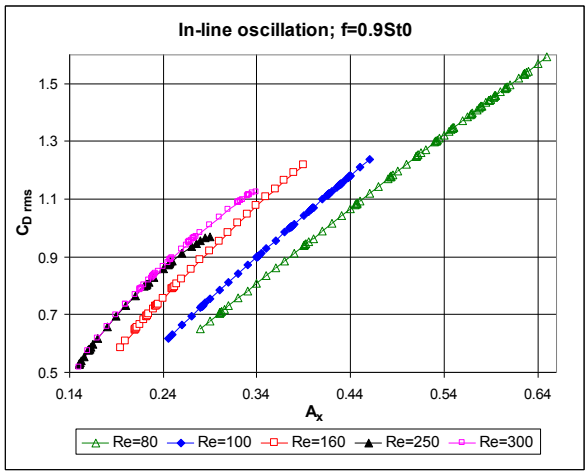

Figure 12. Rms value of drag against amplitude at Re=80, 100, 160, 250, 300

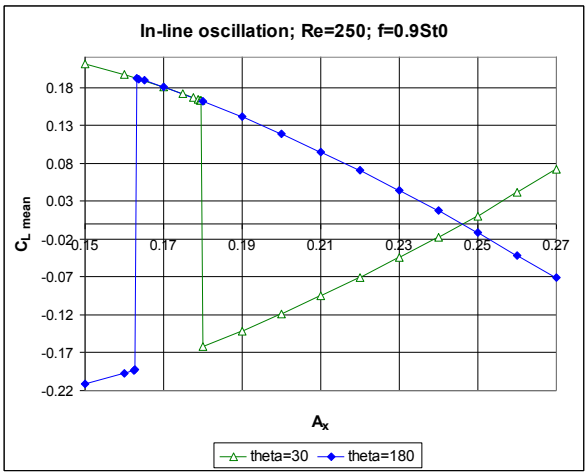

Figure 14. Time-mean of lift versus A_x for initial conditions θ=30° and 180° (Re=250; f / St_0=0.9)

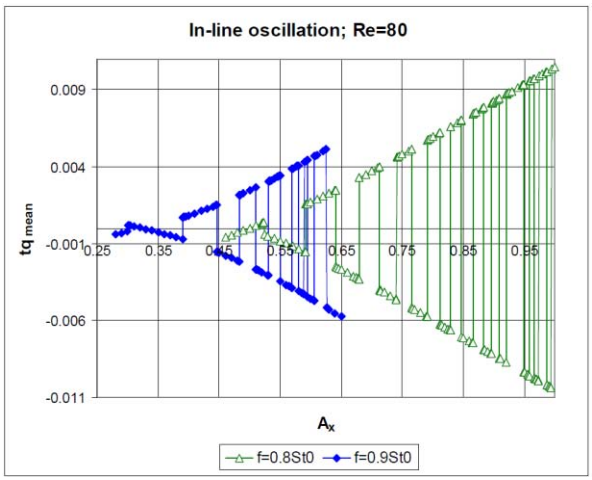

Figure 13. Time-mean of torque versus A_x for frequency ratios of 0.8 and 0.9 (Re=80)

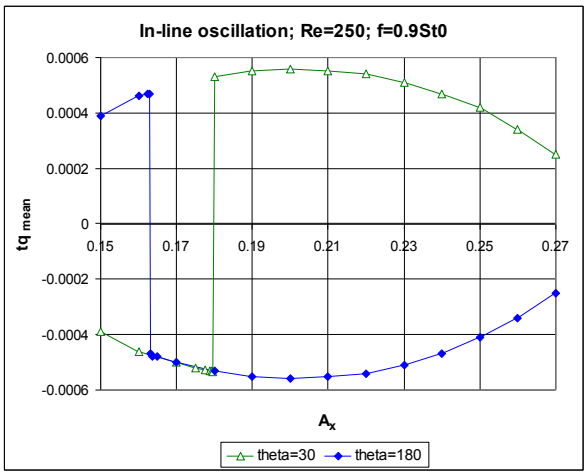

Figure 15. Time-mean of torque versus A_x for initial conditions θ=30° and 180° (Re=250; f / St_0=0.9)

The Effect of Initial Condition

So far all results shown (Figs. 2-13) are from computations for the initial cylinder position of polar angle θ=0° (3 o'clock position). For the case of Re=250 computations were repeated for θ=30°, 45°, 60°, 90° and 180°. Different initial conditions can cause the locations and number of jumps to vary when TM lift and torque coefficients are plotted (Baranyi, 2008), thus reproducing different parts of the state curves. Figures 14 and 15 show the TM lift and torque, respectively, plotted against A_x for θ=30° and 180°. These two values best represent the state curves, which are a mirror image of each other. Interestingly, none of the six θ values investigated resulted in any point on the upper state curve between $0.163 < A_x < 0.18$. This shows how complex the boundary can be which separates the two "basins of attraction" for this nonlinear problem. These results indicate that, at a given amplitude, two mirror-image solutions coexist, sharing solution space, and depending on parameters that include initial condition.

Comparison of Computational Results for Re=200

Computations were carried out for a cylinder oscillated in in-line direction at the resonant frequency f=St$_0$ for Re=200 for different dimensionless amplitude values. Figure 16 shows $(C_L, \dot{C}_L)$ limit cycle curves for different A_x oscillation amplitude values. The figures on the left were obtained by the second and third authors using the commercial software package Ansys CFX based on the finite volume method. The figures on the right were obtained by the first author using an in-house code based on the finite difference method. The agreement between the two sets of results is very good, giving further evidence to the validity of the codes.

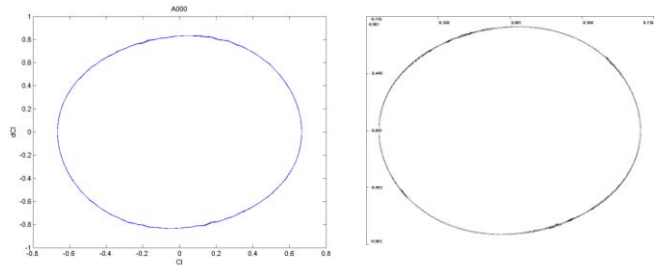

A_x=0

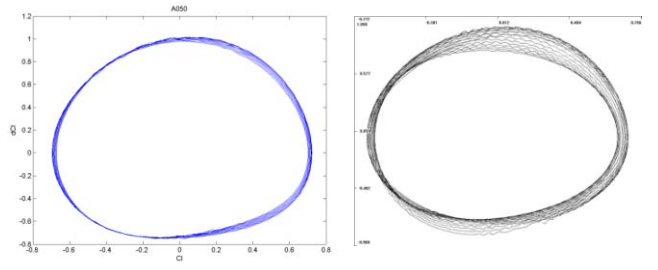

A_x=0.05

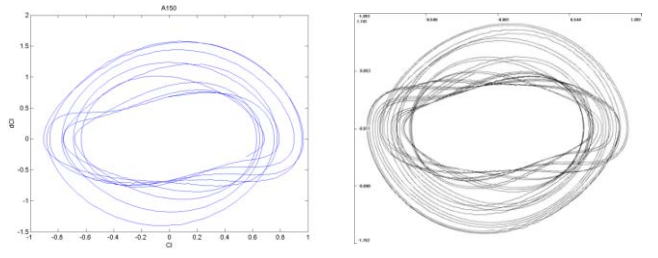

A_x=0.15

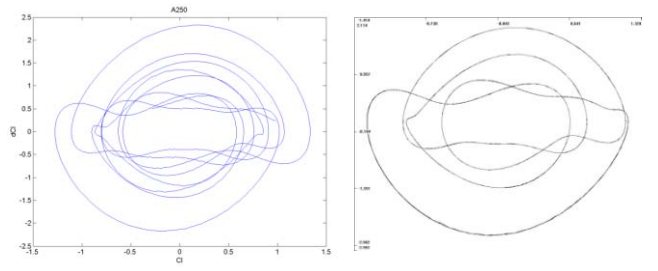

A_x=0.25

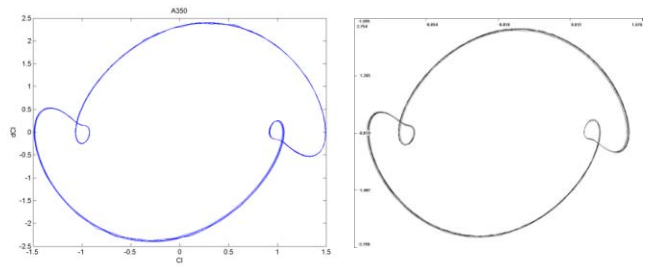

A_x=0.35

Figure 16. $(C_L,\dot{C}_L)$ limit cycle curves for different A_x values (left: CFX; right: In-house code of first author)

Pre- and Post Jump Analysis

The vicinity of a jump is investigated by different means, such as time history of lift, drag-lift limit cycles and vorticity contours. Figure 17 shows a periodic section of the time-history of life for amplitude values directly before and after the jump. The curves appear to be a mirror image of each other.

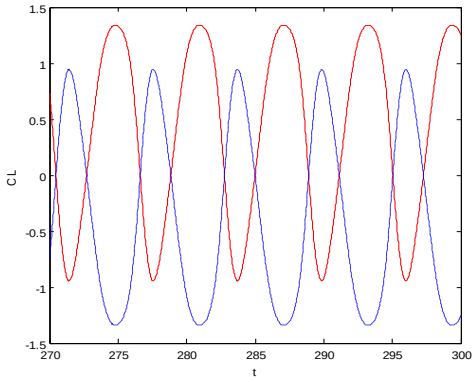

Figure 17. Time history of lift (solid line: A_x=0.2475; dotted line: A_x=0.2478); Re=250

The limit cycle (C_D,C_L) curve shown in Fig. 18 also reveals a mirror image between the pre-jump curve (thick line) and the post-jump curve (thin line). The direction of orientation of the two curves is also opposite.

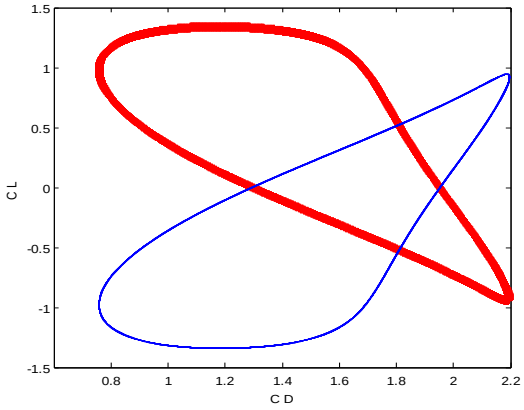

Figure 18. Limit cycle (C_D,C_L); Re=250; f=0.8St$_0$; thick line: A_x=0.2475, thin line: A_x=0.2478

The vorticity contours shown in Fig. 19 also show the mirror image nature of the flow before and after a jump. The gray lines indicate negative vorticity values, and the black are positive. The vortex shedding mode is 1P, meaning that a pair of vortices is shed in one period.

The present cylinder-flow system is reflection symmetric about a line through the cylinder center and parallel to the upstream flow vector. The presence of symmetry in physical systems makes them susceptible to symmetry breaking bifurcations. In the present case, inflow periodic forcing results in a pitchfork bifurcation of the flow – much like the buckling of a beam subjected to axial loading (although much more complex behavior is possible in the dynamic case).

Note that each of the wakes in Fig. 19 by itself no longer has the reflection symmetry on the initial stable flow. Since the overall symmetry must be conserved, the wake flow achieves this by 'generating' reflection symmetric solutions, such that the 'total symmetry' is again conserved if one considers both solutions. This is reflected in Figs. 17-19.

POD Analysis

Figure 20 shows the evolution of the wake flow toward the bifurcated solutions through the lift time-history for two amplitude values on either side of a jump. As can be seen, the two solutions coincide while the wake flow is steady and through one or two fluctuations, but then begin to diverge, becoming more periodic by around *t*=90 (the fully periodic state is shown in Fig. 17).

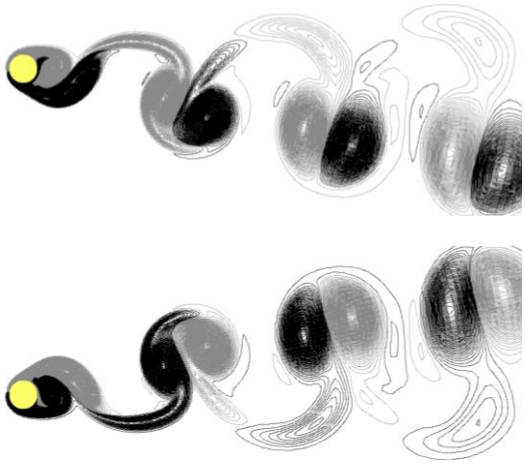

Figure 19. Vorticity contours: top A_x=0.2475; bottom A_x=0.2478 (Re=250; f/St_0=0.8)

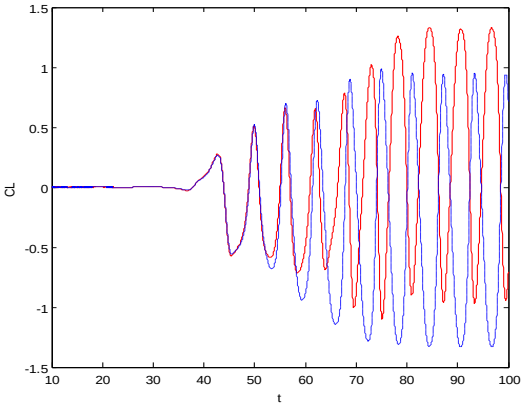

Figure 20. Time history of lift (solid line: A_x=0.2475; dotted line: A_x=0.2478); Re=250, from bifurcation onset

The particular case shown in Figs. 17-20 was also investigated by means of Proper Orthogonal Decomposition (POD) analysis. POD analysis is based on the Karhunen-Loève decomposition. POD is variously known as Principal Component Analysis (PCA) and Singular Value Decomposition (SVD). In POD, space-time data is decomposed into components or modes where the lowest mode carries the most energy, followed by the second etc. The POD decomposition is optimal, meaning that it is the most efficient linear decomposition capturing the highest energy for a given number of modes among all possible linear decompositions (Holmes et al., 1998). Principal modes are extracted from the instantaneous inflow velocity field $u(x,y)$ or the time-varying velocity (excluding the mean) at a given x-location $u(y,t)$. In the analysis, the flow field is projected onto an orthonormal set of spatial functions or modes $\Psi_k(x,y)$ in the former case, and $\Psi_k(y,t)$ in the latter. For the spatial decomposition, for instance, the u-velocity field may be expressed as the modal superposition

$$u(x,y) = \sum_{k=1}^{r} a_k \Psi_k(x,y)$$

POD analysis makes it possible to 'visualize' the flow based on only a few of the most important modes. It is then easier to uncover the detailed dynamics of the wake. Spatial POD modes based on the inflow and transverse flow velocity components were computed for the two cases shown in Fig. 17 for the spatial decomposition and Fig. 20 for the spatial-temporal decomposition.

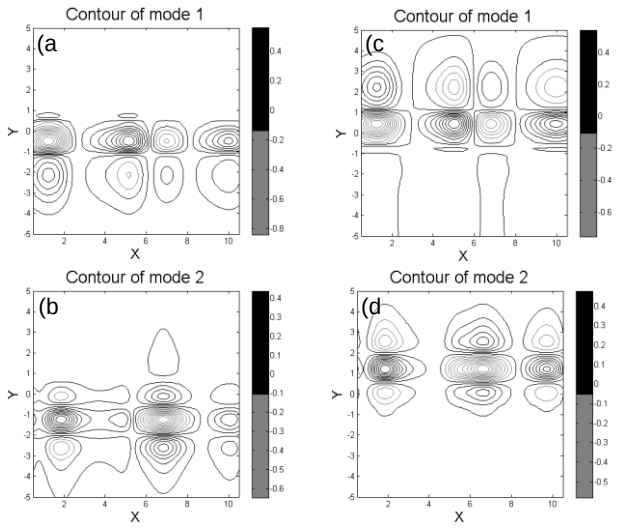

Figure 21. Spatial POD modes 1 and 2, before the jump (a,b), A_x=0.2475, and after the jump (c,d) A_x=0.2478; Re=250.

The spatial POD modes, Fig. 21, show the clear preference of the flow to shed upward or downward due to the broken the cylinder centerline reflection symmetry. The symmetry relation between the individual modes for the two cases is also striking. This strongly supports the proposed idea of a pitchfork bifurcation of the wake as the underlying governing mechanism

of the wake transition. Although not shown for brevity, all higher modes show the same symmetry relation.

Spatio-temporal POD computations were also performed, in the case shown here, for the velocity component $u(y,t)$ parallel to the upstream flow velocity vector associated with the time evolution of the flow shown in Fig. 20. The evolution of the first two temporal POD modes is shown in Fig. 22. The time scale corresponds to that of Fig. 20. One clearly identifies the instance near t=60 where the unstable symmetrical wake switches into the stable asymmetrical state. Fig. 22 also sheds some light on how the wake actually makes the transition from the unstable to the stable state. Notice that at t=60 the first mode briefly 'disappears' while coincidentally mode 2 is briefly dominant. At t=65 the first recovers the energy but is now asymmetrical while the mode 2 energy decreases but its frequency is clearly higher. The result is a complete change in the flow structure and frequency starting near t=60.

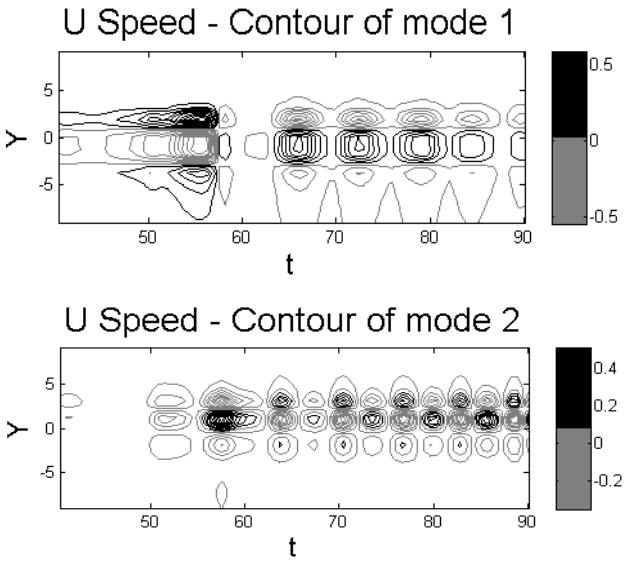

Figure 22. Temporal evolution of U-velocity POD modes 1 and 2, for A_x=0.2478; Re=250.

While all modes were found to undergo transition at approximately the same time (here near t=60), the two modes presented here capture the key wake transition dynamics. Based on the POD singular values, these modes carry over 95% of the 'energy'. The foregoing brief presentation on POD analysis shows the potential for the approach as a tool for in-depth 'visualization' of the wake dynamics. The analysis can even be carried further. POD modes provide the capability to represent the flow a small number of modes in a low order model as have been done, for instance, by Mureithi et al. (2009). Their POD based low order model made possible an in-depth study of the wake dynamics for the case of Re=200 presented in Fig. 16 here. In particular, the simple model could reproduce the observed bifurcations including the chaotic state and period-doubling bifurcation for large forcing amplitudes.

CONCLUSIONS

This computational study deals with a systematic investigation of flow around a cylinder forced to oscillate in-line with the main stream. Nine Reynolds numbers (from Re=60-350) and two frequency ratios are considered, and time-mean (TM) and rms values of force coefficients were plotted against oscillation amplitude A_x.

- With increasing Re at a fixed frequency ratio, the general trend was that both TM and rms curves shifted to smaller A_x values.
- With the higher frequency ratio of 0.9, all TM and rms curves shifted to smaller A_x values.
- Jumps between two solutions were found in all cases for the TM of lift and torque.
- Post-jump solutions are mirror images of pre-jump solutions.
- POD analysis confirms that the reflection-symmetry relation is present at all orders and between individual modes. The temporal POD modes also show the transition of the wake flow to the bifurcated state.

In this study only two frequency ratios were investigated, due to the huge amount of computational work involved. Further investigation on the effect of frequency ratio is needed.

ACKNOWLEDGMENTS

The support provided by the Hungarian Research Foundation (OTKA Project Nos. K 76085 and K 68207) is gratefully acknowledged by the first author. The authors thank Mr. L. Daróczy for designing the flow visualization software. The support of NSERC is gratefully acknowledged by the last two authors.

REFERENCES

Al-Mdallal, Q.M., Lawrence, K.P. and Kocabiyik, S., 2007, "Forced streamwise oscillations of a circular cylinder: Locked-on modes and resulting fluid forces," *Journal of Fluids and Structures* **23**, 681-701.

Baranyi, L., 2008a, "Numerical simulation of flow around an orbiting cylinder at different ellipticity values," *Journal of Fluids and Structures* **24**, 883-906.

Baranyi, L., 2008b, "Effect of frequency ratio on the force coefficients of a cylinder oscillated in a uniform stream," *Proc. 7th JSME-KSME Thermal and Fluids Engineering Conference*, Sapporo, Japan, Paper No. L132.

Baranyi, L., 2009, "Sudden and gradual alteration of amplitude during the computation for flow around a cylinder oscillating in transverse or in-line direction," *ASME 2009 Pressure Vessels and Piping Conference, Symposium on Flow-Induced Vibration*. Prague, Paper No. PVP2009-77463.

Blackburn, H.M. and Henderson, R.D., 1999, "A study of two-dimensional flow past an oscillating cylinder," *Journal of Fluid Mechanics* **385**, 255-286.

Cetiner, O. and Rockwell, D., 2001, "Streamwise oscillations of a cylinder in a steady current. Part 1. Locked-on states of vortex formation and loading," *Journal of Fluid Mechanics* **427**, 1-28.

Chakraborty, J., Verma, N. and Chhabra, R.P., 2004, "Wall effects in flow past a circular cylinder in a plane channel: a numerical study," *Chemical Engineering and Processing* **43**, 1529–1537.

Chen, M.M., Dalton, C. and Zhuang, L.X., 1995, "Force on a circular cylinder in an elliptical orbital flow at low Keulegan-Carpenter numbers," *Journal of Fluids and Structures* **9,** 617-638.

Didier, E. and Borges, A.R.J., 2007, "Numerical predictions of low Reynolds number flow over an oscillating circular cylinder," *Journal of Computational and Applied Mechanics* **8**(1), 39-55.

Holmes, P., Lumley, J.L., and Berkooz, G., 1998, Turbulence, Coherent Structures, Dynamical Systems and Symmetry, Cambridge University Press.

Kaiktsis, L., Triantafyllou, G.S. and Özbas, M., 2007, "Excitation, inertia, and drag forces on a cylinder vibrating transversely to a steady flow," *Journal of Fluids and Structures* **23**, 1-21.

Konstantinidis, E., Balabani, S. and Yianneskis, M., 2005, "The timing of vortex shedding in a cylinder wake imposed by periodic inflow perturbations," *Journal of Fluid Mechanics* **543**, 45-55.

Kravchenko, A.G., Moin, P. and Shariff, K., 1999. "B-Spline method and zonal grids for simulations of complex turbulent flows," *Journal of Computational Physics* **151**, 757–789.

Lu, X.Y. and Dalton, C., 1996, "Calculation of the timing of vortex formation from an oscillating cylinder," *Journal of Fluids and Structures* **10**, 527-541.

Mureithi, N.W., Huynh, K. and Pham, A., "Low order model dynamics of the forced cylinder wake," *ASME 2009 Pressure Vessels and Piping Conference, Symposium on Flow-Induced Vibration*. Prague, (2009), Paper No. PVP2009-78093

Norberg, C., 2003, "Fluctuating lift on a circular cylinder: review and new measurements," *Journal of Fluids and Structures* **17**, 57-96.

Posdziech, O. and Grundmann, R., 2007, "A systematic approach to the numerical calculation of fundamental quantities of the two-dimensional flow over a circular cylinder," *Journal of Fluids and Structures* **23**, 479-499.

Williamson, C. H. K. and Roshko, A., 1988, "Vortex formation in the wake of an oscillating cylinder," *Journal of Fluids and Structures* **2**, 355-381.